

# Preliminary experimental results by the prototype of Sanya Incoherent Scatter Radar

XinAn Yue<sup>1,2,3,4\*</sup>, WeiXing Wan<sup>1,2,3,4</sup>, Han Xiao<sup>1,2,3,4</sup>, LingQi Zeng<sup>1,2,3\*</sup>, ChangHai Ke<sup>5</sup>, BaiQi Ning<sup>1,2,3</sup>, Feng Ding<sup>1,2,3,4</sup>, BiQiang Zhao<sup>1,2,3,4</sup>, Lin Jin<sup>5</sup>, Chen Li<sup>5</sup>, MingYuan Li<sup>1,2,3,4</sup>, JunYi Wang<sup>1,2,3</sup>, HongLian Hao<sup>1,2,3</sup>, and Ning Zhang<sup>1,2,3</sup>

<sup>1</sup>Key Laboratory of Earth and Planetary Physics, Institute of Geology and Geophysics, Chinese Academy of Sciences, Beijing 100029, China;

<sup>2</sup>Innovation Academy for Earth Science, Chinese Academy of Sciences, Beijing 100029, China;

<sup>3</sup>Beijing National Observatory of Space Environment, Institute of Geology and Geophysics, Chinese Academy of Sciences, Beijing 100029, China;

<sup>4</sup>College of Earth and Planetary Sciences, University of the Chinese Academy of Sciences, Beijing 100049, China;

<sup>5</sup>Nanjing Research Institute of Electronics Technology, Nanjing 210039, China

## Key Points:

- A prototype of Sanya Incoherent Scatter Radar consisting of 8 subarrays (SYISR-8) has been developed for technical test purpose
- The technical details of SYISR-8 were described and the amplitude and phase among 256 channels were calibrated
- The SYISR-8 is able to detect space station, tropospheric wind and meteor quite well

**Citation:** Yue, X. A., Wan, W. X., Xiao, H., Zeng, L. Q., Ke, C. H., Ning, B. Q., Ding, F., Zhao, B. Q., Jin, L., Li, C., Li, M. Y., Wang, J. Y., Hao, H. L. and Zhang, N. (2020). Preliminary experimental results by the prototype of Sanya Incoherent Scatter Radar. *Earth Planet. Phys.*, 4(6), 579–587. <http://doi.org/10.26464/epp2020063>

**Abstract:** In the past decades, the Incoherent Scatter Radar (ISR) has been demonstrated to be one of the most powerful instruments for ionosphere monitoring. The Institute of Geology and Geophysics at the Chinese Academy of Sciences was founded to build a state-of-the-art phased-array ISR at Sanya (18.3°N, 109.6°E), a low-latitude station on Hainan Island, named the Sanya ISR (SYISR). As a first step, a prototype radar system consisting of eight subarrays (SYISR-8) was built to reduce the technical risk of producing the entire large array. In this work, we have summarized the preliminary experimental results based on the SYISR-8. The amplitude and phase among 256 channels were first calibrated through an embedded internal monitoring network. The mean oscillation of the amplitude and phase after calibration were about 1 dB and 5°, respectively, which met the basic requirements. The beam directivity was confirmed by crossing screen of the International Space Station. The SYISR-8 was further used to detect the tropospheric wind profile and meteors. The derived winds were evaluated by comparison with independent radiosonde and balloon-based GPS measurements. The SYISR-8 was able to observe several typical meteor echoes, such as the meteor head echo, range-spread trail echo, and specular trail echo. These results confirmed the validity and reliability of the SYISR-8 system, thereby reducing the technical risk of producing the entire large array of the SYISR to some extent.

**Keywords:** incoherent scatter radar; SYISR; ionosphere; phased array; beam direction; tropospheric wind; meteor

## 1. Introduction

In 1958, Dr. W. E. Gordon from Cornell University first proposed that the ionosphere could be measured by means of ground-based high-powered radar through electron Thomson scattering (Thomson, 1906; Gordon, 1958). He thought that the Thomson scattering from different electrons was incoherent and named this new technology Incoherent Scatter Radar (ISR). Soon after, Dr. K. L. Bowles from the National Bureau of Standards successfully observed the first incoherent scattering signal from the ionosphere after a short period of technical preparation (Bowles, 1958). In the

experiment, he found that the measured power spectrum width and Doppler shift were much smaller than predicted by electron incoherent scattering theory, which implied that the observed signal was not totally incoherently scattered from free electrons. After that, a variety of theoretical studies were done on the ISR (Dougherty and Farley, 1960; Hagfors, 1961; Kudeki and Milla, 2011). It is now accepted that the measured signal of the ISR is actually partially coherent owing to the Coulomb force of ions on electrons. But the term “incoherent scatter” continues to be used by the community today.

After the pioneering ionospheric incoherent scatter experiment by Bowles in 1958 (Bowles, 1958), the United States quickly built several famous ISRs in the 1960s, including those located at Jicamarca, Arecibo (Cohen, 2009), Millstone Hill, and Søndre Strømfjord, the majority of which are still in operation today. Sub-

Correspondence to: X. A. Yue, [yuexinan@mail.iggcas.ac.cn](mailto:yuexinan@mail.iggcas.ac.cn)

L. Q. Zeng, [zlg@mail.iggcas.ac.cn](mailto:zlg@mail.iggcas.ac.cn)

Received 26 MAY 2020; Accepted 16 JUN 2020.

Accepted article online 27 AUG 2020.

©2020 by Earth and Planetary Physics.

sequently, other countries or regions of the world gradually established their own ISRs, such as the Kharkov radar by the former Soviet Union, the MU radar by Japan (Fukao et al., 1985), and the European Incoherent SCATter facility (EISCAT; Röttger et al., 1995). These ISRs have differences in frequency, peak power, antenna type and geometry, pulse width, and their main scientific purpose. Most of the ISRs mentioned above have the disadvantage of being unable to operate continuously for a long time because they use massive antenna structures and powerful centralized transmitters. To resolve this issue, the United States began to build a new class of phased-array modular design ISRs with a large number of identical electronic subsystems, recently named the Advanced Modular Incoherent Scatter Radar (AMISR; Valentic et al., 2013). It has the advantages of instantaneous pulse-to-pulse beam steering, remote accessibility for observing operations, and the ability to tolerate hardware failures of individual antenna element units. To date, the United States has built two AMISRs, named the Poker Flat ISR (PFISR) and the Resolute Bay ISR (RISR). Additionally, the Europeans are making great efforts to develop an updated version of their current multistatic radar system, which will be called the EISCAT-3D (McCrea et al., 2015). This new radar system will also use phased arrays with advanced software and data processing techniques. It will be able to do volumetric imaging, aperture synthesis imaging, auto tracking, and adaptive experiments, which will give the radar higher sensitivity and resolution, greater flexibility, and better continuity and reliability. It is expected that the system will promote radar techniques and new methods for coding and analysis and will advance our scientific understanding of atmospheric physics and global change, space and plasma physics, space weather and service applications, and even solar system research.

In China, some ionospheric incoherent scattering experiments have been performed using high-powered military radar in the early stages of development. In 2014, the China Research Institute of Radio-Wave Propagation reengineered an outdated radar system to detect the ionosphere the same as an ISR (Ding ZH et al., 2018). Subsequently, in 2015, the National Natural Science Foundation of China founded the Institute of Geology and Geophysics at the Chinese Academy of Sciences to develop a state-of-the-art ISR in Sanya (18.3°N, 109.6°E), a low-latitude station on Hainan Island. The main technical features of the Sanya ISR (SYISR) include modular active electronic scanning, a digital phased array, all solid-state transmitting, and digital receiving. It is expected to be one of the most important ISRs in East Asia and the only one with the capability of operating continuously at low latitude once it is completed. The anticipated scientific objectives include, but are not limited to, a better understanding of the low-latitude atmosphere–ionosphere–magnetosphere coupling, regional characteristics of the ionosphere in East Asia, and ionospheric scintillation in the low-latitude region.

Because this is our first experience with building a phased-array ISR in China, we have worked out a step-by-step construction plan to minimize potential technical risks that could arise when building the entire array at one time. As a first step, we built a prototype of the SYISR in 2018 to conduct a number of technical tests. For nearly 2 years, the SYISR has been working on the basis of

case-by-case experiments under different configurations. Using this prototype, we have completed several scientific experiments, such as profiling the tropospheric wind and detecting the meteor echoes. In Section 2, we introduce the technical details of the prototype SYISR. In Section 3, we present the preliminary experimental results. We then conclude the paper and indicate the next steps in Section 4.

## 2. The Prototype of Sanya Incoherent Scatter Radar

The prototype SYISR is located near the city of Nanjing (32°N, 119°E) in Jiangsu Province. It consists of eight subarrays, as illustrated in Figure 1, and is therefore referred to as SYISR-8. Note that as designed, the SYISR will have 128 subarrays in total, which means that the SYISR-8 has one sixteenth of the full radar power. Each subarray includes 1 transmitter power supply, 1 receiver power supply, 1 subarray excitation device, 2 power dividers, 32 transmitter/receiver (T/R) units, and 32 antennas. Figure 2 shows both top and bottom views of the structural subarray. As illustrated, it is a phased array with a triangular grid and rectangular boundary. This is an optimized design, with comprehensive consideration given to radar gain, unit number, and field area. The antenna was designed to be connected directly to the T/R unit to reduce the power loss through a cable. Furthermore, each subarray has an internal monitoring network for the purpose of monitoring and calibrating the amplitude and phase of each channel. In addition to the antenna array shown in Figure 1, the entire prototype system includes several cabinets consisting of power suppliers, a pre-transmitter amplifier, frequency integration, computers, and control units, which are integrated into two shelters (not shown here). Table 1 summarizes the main parameters of the SYISR-8. Note that some parameters, such as the peak power, antenna aperture, and beam width, are different from the final SYISR because of the difference in array size.

The SYISR will be operating at Sanya, a low-latitude seaside station, where the environment frequently experiences high temperatures, high salt, and high humidity. It is therefore crucial for each piece of radar equipment to be well suited to these extreme conditions. Of all the SYISR components, the T/R unit is definitely the key part that must meet this requirement. In addition to considering this environmental requirement in the design phase, the T/R



**Figure 1.** The appearance of the SYISR-8.

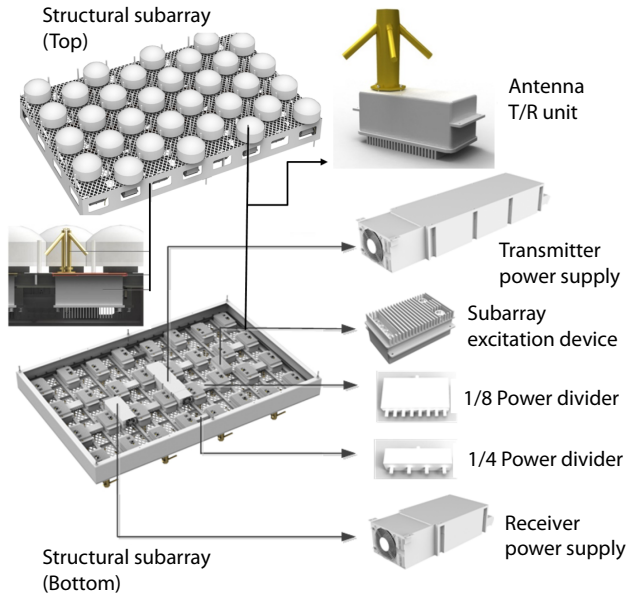


**Figure 2.** Schematic diagram of the subarray structure from both the top and bottom. Note that each subarray has 1 transmitter power supply, 1 receiver power supply, 1 excitation device, 2 power dividers, and 32 antennas and T/R units.

unit was tested in the laboratory after production under extreme temperature, salt, and fog conditions, as illustrated in the left panel of Figure 3. The working status, humidity, and corrosion of the T/R unit were monitored and compared to ensure the unit worked well under different conditions.

To test the performance of the antenna unit, we built an indoor passive small array system consisting of  $5 \times 5$  antenna units aligned the same as the SYISR design. The middle panel of Figure 3 shows the appearance of this passive array and test configuration inside a microwave room. The wide-angle scanning characteristic, stationary wave characteristic, and radiation pattern of the antenna were monitored and confirmed.

We further built an indoor active system to test the performance

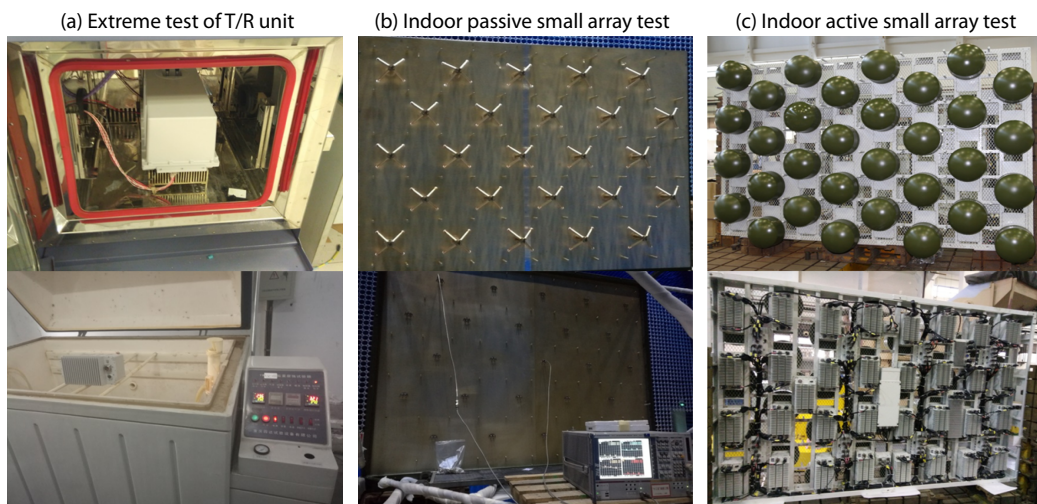


**Figure 3.** (Left) Indoor test of the T/R unit under an extreme temperature and salt-fog environment. (Middle) Indoor passive small array test. (Right) Indoor active small array test.

**Table 1.** SYISR-8 radar characteristics.

Parameter	Value and description
Frequency	$440 \pm 10$ MHz
Peak power	128 kW
Antenna aperture	$6 \times 8$ m
Antenna type	Cross dipole, circular polarization, phased array
T/R units	Solid state, 500 W each, 256 units in total
Beam width	$\sim 4.3^\circ \times 5.7^\circ$
Sampling frequency	4 MHz
System noise temperature	$\leq 120$ K
Duty cycle	$\leq 10\%$
Pulse form	Designable, e.g., uncoded pulse, linear frequency modulation, Barker code, etc.

of the subarray. The right panel of Figure 3 displays the front and rear views of this system. Its components and layout are exactly the same as each subarray of the SYISR, as illustrated in Figure 2. The transmitting and receiving lobes of this system were measured to determine the beam width and gain. The reliability and stability were confirmed through 60 hours of continuous operation with a 3% duty cycle. For each T/R unit, an active stationary wave was tested by a mutual coupling method.

### 3. Preliminary Experimental Results

The peak power of the current SYISR-8 is 128 kW, which is not strong enough to measure the very weak incoherent scatter signal of the ionosphere. However, the SYISR-8 instrument has sufficient power to potentially receive a coherent echo from the lower atmosphere and track meteor phenomena in the middle and upper atmosphere. These measurements can test the stability of the radar's electrical and operational system and thereby minimize the technical risk of producing the entire array. In the following

section, we describe in detail the experimental results of the amplitude and phase consistency calibration, the beam direction confirmation, tropospheric wind profiling, and meteor observations, respectively.

### 3.1 Amplitude and Phase Consistency Calibration

The consistency of amplitudes and phases among different channels is the key factor that determines the performance of the phased-array radar (Kuehnke, 2001; Fulton and Chappell, 2009; Liu JX et al., 2011). This can affect the sum and difference beams and should be monitored and calibrated before conducting any experiment. For SYISR-8, this was done in a microwave room by using the internal monitoring network embedded in the antenna array. Specifically, for the transmitting channel, we first set all active channels of the small array to the transmitting state and the phase shifter to a zero state. A radio frequency signal generated by a vector network analyzer was then injected into the array through the internal monitoring network. The transmitting channel was controlled to open with the control system, and the corresponding amplitude and phase were monitored sequentially by the data acquisition system. The amplitude and phase calibration values for each channel were then obtained and the firmware was updated. A planar near-field test system was used to measure the transmitting lobe to evaluate the calibration effect. This step can be repeated for different frequencies. For the receiving channel, the procedure was almost the same as that for the transmitting channel, except that the array was set to a receiving state during the calibration process.

As an example, Figure 4 shows the amplitude and phase oscillations among all 256 channels of SYISR-8 for both the transmitting and receiving channels after an indoor calibration process. We can see that the mean oscillation amplitude of both the transmitting and receiving channels was about 1 dB, whereas it was about  $5^\circ$  for the phase. These values met the basic requirements of digital beam forming and were acceptable to us.

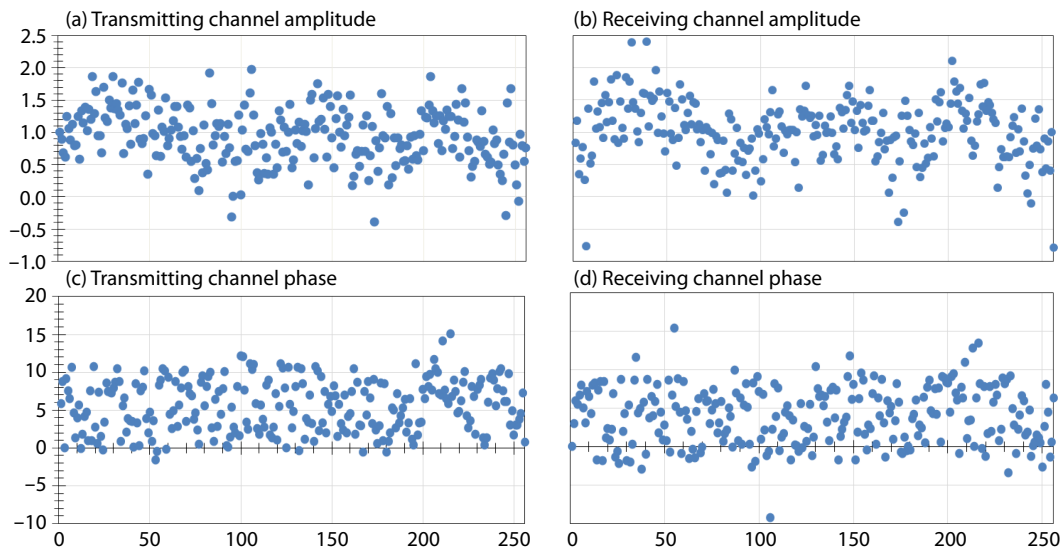


**Figure 4.** (Top) Amplitude (dB) and (bottom) phase (degree) oscillations among 256 channels of the SYISR-8 after calibration. (a, c) Transmitting channels; (b, d) receiving channels. The numbers on the x-axis indicate the channel order.

To further show the effect of this calibration process, we plotted an example of the lobes received by SYISR-8 for the sum beam and difference beam before and after phase calibration along the normal direction of the radar, as shown in Figure 5. We can see that the antenna pattern was improved significantly by the calibration process. For example, the sum and difference beams had better symmetry after calibration. The zero depth of the difference beam was much deeper after calibration.

### 3.2 Beam Direction Confirmation

The beam directivity of the SYISR-8 could not be confirmed by traditional methods, such as a near-field tower, because of its geometry of facing the zenith direction (Mailloux, 2005). We used the satellite crossing screen method in the study to confirm the beam direction. The selected satellite was the International Space Station (ISS) because of its relatively large scattering cross section and therefore better signal-to-noise ratio. The beam direction made by digital beam forming was obtained from a theoretical simulation. It was then set up toward a constant direction through which the ISS would pass, according to orbital prediction based on its two-line element file. When the ISS crossed the beam, the corresponding amplitude and phase of the sum and difference beams were observed. The polarity and amplitude ratio of the sum and difference beams were analyzed to confirm the accuracy of the beam direction. The specific parameters used in this experiment are given in Table 2.

Figure 6 shows the polarity curve and amplitude ratio curve of the sum and difference beams for both the elevation plane and azimuth plane during the interval when the ISS crossed the beam of the SYISR-8. We can see clearly from both curves that the ISS first enters the beam, crosses the center of the beam, and then flies to the other side of the beam. The time at which the ISS was located in the center of the beam could be derived. By comparing the predicted beam and ISS orbital parameters, we confirmed the beam directivity of the SYISR-8.

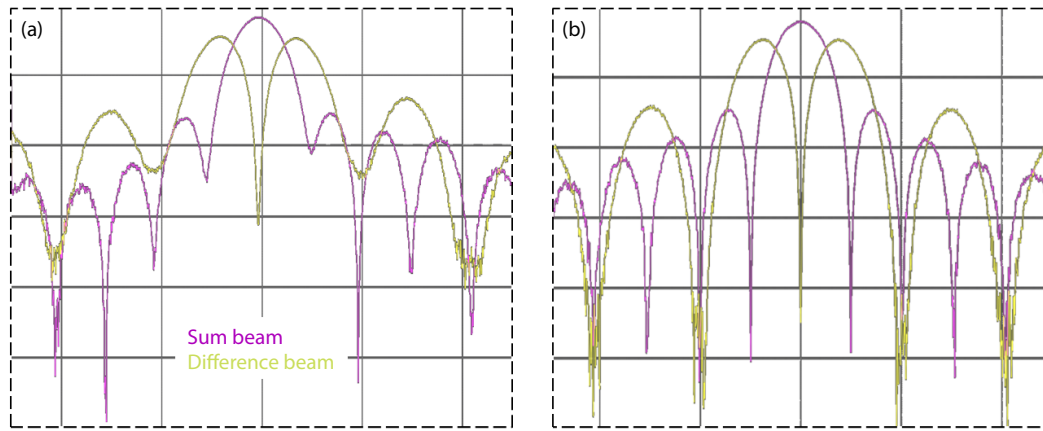


**Figure 5.** Example of the received lobes of the sum beam (purple) and difference beam (yellow) along a normal direction before (a) and after (b) phase calibration by the SYISR-8. Each interval along the y-axis represents 10 dB.

**Table 2.** SYISR-8 configurations for experiments on beam direction confirmation, tropospheric wind detection, and meteor detection.

Parameter	Beam direction experiment	Wind experiment	Meteor experiment
Pulse width	500 $\mu$ s	2 $\mu$ s	200 $\mu$ s
Pulse repetition interval	16.667 ms	350 $\mu$ s	6.6 ms
Bandwidth	4 MHz	0.5 MHz	4 MHz
Pulse form	Linear frequency modulation	Uncoded pulse	Linear frequency modulation
Duty cycle	3%	0.57%	3.03%
Beam direction	Steerable	Zenith, 15° off-zenith to the east, west, south, and north	Perpendicular to B at 100 km
Number of coherent integration	1	25	1
Monitoring altitude	>300 km	1.5–32.7 km	60–150 km
Range resolution	~37.5 m	~300 m	~37.5 m

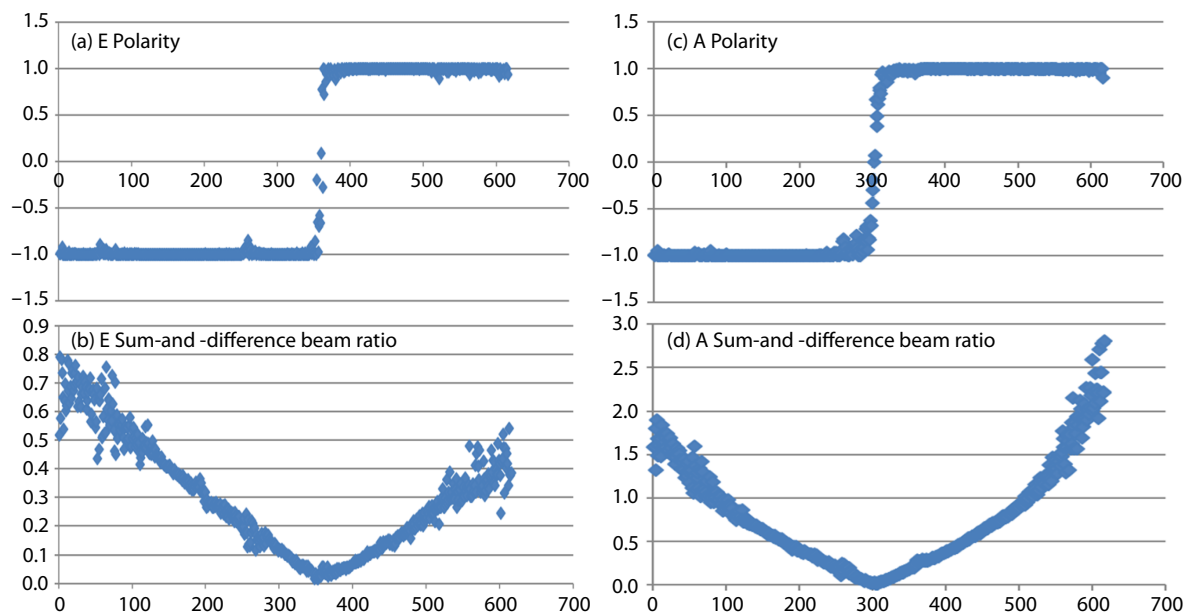


**Figure 6.** (Top) Polarity curve and (bottom) amplitude ratio curve of the sum and difference beams for the (left) elevation plane and (right) azimuth plane, respectively, during the interval when the International Space Station crossed the screen. The numbers on the x-axis indicate the sampling points. The results for the elevation plane and azimuth plane are from different cases.

### 3.3 Profiling the Tropospheric Wind

Tropospheric wind monitoring plays an important role in numerical weather prediction and atmospheric science (Benjamin et al., 2004). Traditionally, tropospheric wind has been measured by a variety of technologies, including lidar, a global navigation satellite system, and wind profiler radar, among others. Both the frequency and power of the SYISR-8 are comparable with the frequently used tropospheric wind profiler radar in the very high frequency band (Lindseth et al., 2012). This fact enabled us to evaluate the SYISR-8 by measuring the tropospheric wind on the basis of Bragg scattering (Röttger and Liu CH, 1978).

We configured the SYISR-8 to be able to detect the troposphere by traditional wind profiler radar. Table 2 specifies the setup of the radar and signal processing parameters in detail. We set up five beams with directions of east, west, north, south, and zenith, respectively. We made measurements for 30 s in each direction, and one observational cycle completed observations in all five directions. Several experiments were done so as to include both sunny and rainy days. To explore the effect of the seasonal variation in turbulence intensity on the returned echoes, we conducted experiments during June/July and October/November of 2019.

We used a common method to retrieve the neutral wind from the wind profiler radar (Strauch et al., 1984). Specifically, the observed I/Q signal was processed to obtain the power spectral density by averaging the echo signal in the time domain, removing the direct current, conducting a fast Fourier transform spectrum analysis, obtaining the spectral average, calculating the noise reduction, removing the ground clutter, and other steps. As an example, Figure 7 shows the spectral density versus altitude and frequency shift from the east beam 15° off the zenith observed during the

summer and winter, respectively. As shown in the figure, effective echoes could be observed up to ~9 km in summer and ~5 km in winter. The difference was probably due to the seasonal difference in turbulence intensity. On the basis of this power spectral density data, the echo signal was identified and the spectral moment was extracted to obtain the echo power intensity, radial velocity, spectral width, and other information. Figure 8 shows the corresponding Doppler radial velocity of five beams made on July 30, 2019, around local time 10:00. The radial velocity of the four tilted beams ranged from about -5 to 5 m/s. The zenith beam showed much smaller radial velocity and ranged from -0.5 to 0.5 m/s. This result indicates that the vertical wind is much smaller than the horizontal wind. From both the spectral and radial velocity, we could see that the results for the east (north) and west (south) beams were almost symmetrical with respect to the zero value, implying good data quality and atmospheric stability in this case. Under the assumption of a uniform local wind field, the wind velocity and direction could be solved by the combination of the radial velocity of different beams.

The consistency was evaluated first by comparing winds in the same direction but from different combinations of radio beams. We further compared the wind results with dedicated balloon-based global positioning system (GPS) and co-located radiosonde results. Figure 9 shows a comparison example of the horizontal wind velocity and direction among the SYISR-8, balloon-based GPS launched at the same location for evaluation purpose, and co-located radiosonde in Nanjing. The distance between the SYISR-8 and the radiosonde was about ~40 km. Note that the balloon will drift from the release location with time because of the effect of the horizontal wind. If a local wind gradient exists, a difference will be observed among the three methods. The time of

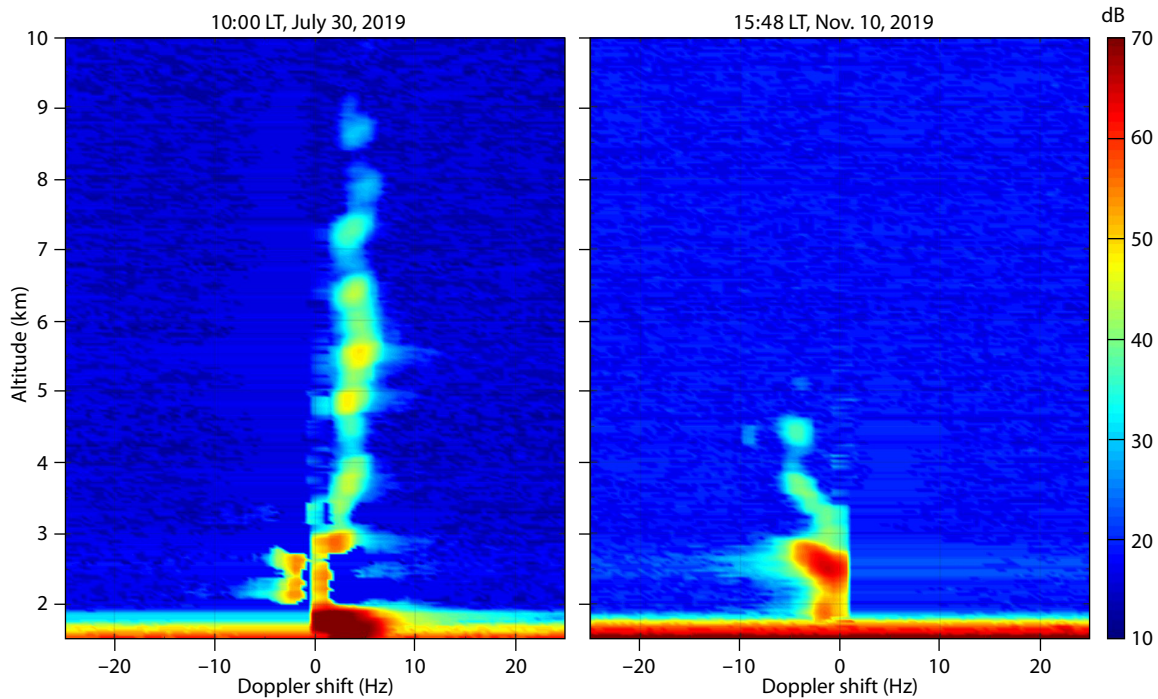


**Figure 7.** Example echo spectrum of the beam 15° off the zenith to the north made by the SYISR-8 around local time (LT) 10:00 on July 30, 2019 (left) and LT 15:48 on November 10, 2019 (right).

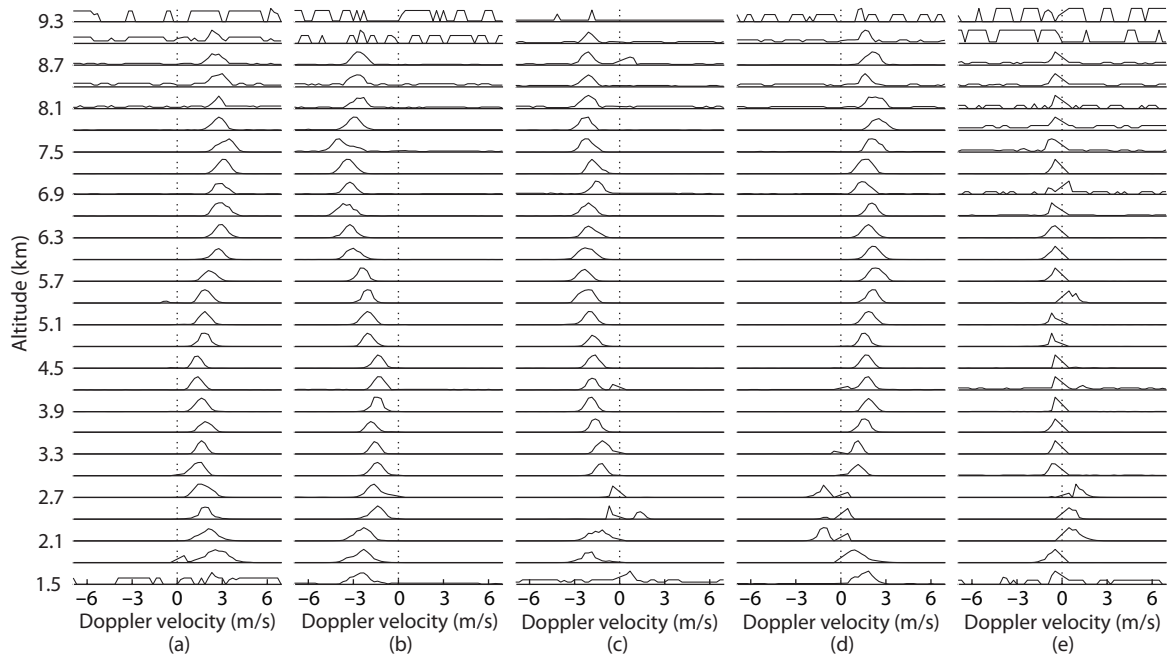


**Figure 8.** Doppler velocities versus altitude of five beams measured by the SYISR-8 at local time 10:00–10:02 on July 30, 2019. The results from (a) to (e) are for the east, west, south, and north oblique beams and zenith beam, respectively.

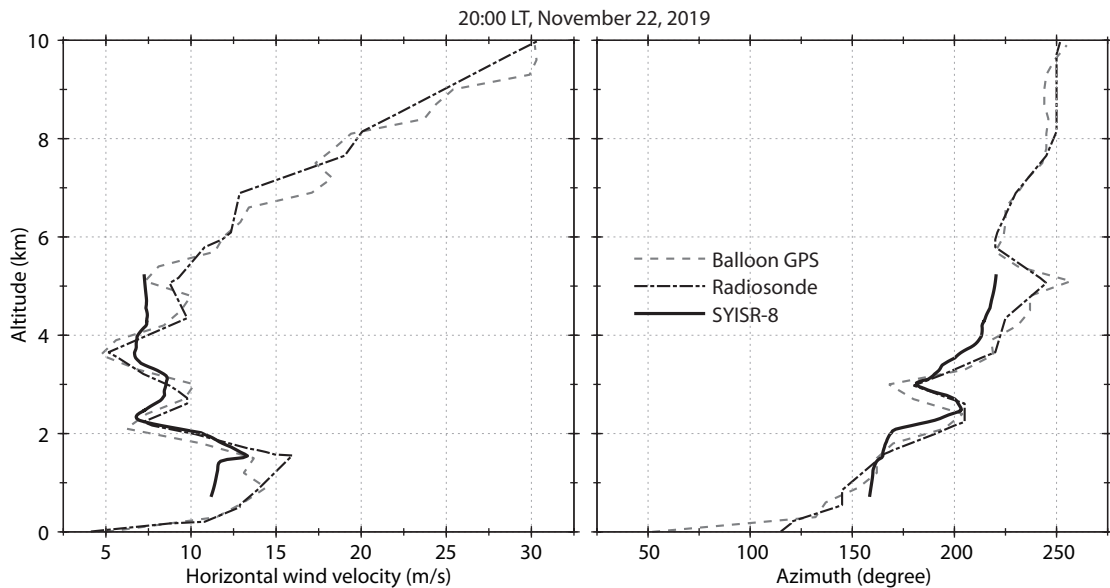


**Figure 9.** Comparison of horizontal wind velocity (left) and azimuth angle (right) measured by balloon-based GPS (dashed lines), co-located radiosonde (dashed and dotted lines) and the SYISR-8 (solid lines) on November 22, 2019, around local time (LT) 20:00.

the experiment was November 22, 2019, around local time 20:00. First, we can see that the effective wind measurement of the SYISR-8 was up to ~7 km, which is lower than the other two methods. Overall, they showed similar altitude variations. Some minor differences did exist among the three methods. This was probably due to the existence of local wind gradients. We also obtained statistics for five cases that had both SYISR-8 and radiosonde measurements during November 2019. These results indicated that the SYISR-8 could be used for wind profiling with reliable accuracy, and they further proved the validity of the technical design of the SYISR to some extent.

### 3.4 Observing Meteors

Although meteors are only occasionally visible to the human eye, micrometeoroids with a microgram to milligram mass are injected into the earth’s atmosphere almost all the time. The meteorite material enters the earth’s atmosphere at a high speed of 11–72 km/s, which generates a high temperature and plasma through ablation and fragmentation (Zhou QH et al., 2001; Mathews et al., 2008). Meteors provide a natural laboratory for studying this intense physical phenomenon. The material and energy left by the meteor through ablation could significantly affect the upper atmosphere. Meteors are one of the causes of ionospheric

irregularity. It is believed that the formation of the E<sub>s</sub> layer and occasionally a metal layer is directly related to the injection of meteors. Meteoroids also pose an existential threat to human space activities. Therefore, observing meteors is of great significance to scientific research and space safety.

Ground-based optical and radio techniques are currently the main means of observing meteors (Zeng LQ and Yi F, 2011). High-power large-aperture radar can detect the ablation process of micrometeors at a high resolution. The ISRs of MU, Arecibo, Jicamarca, AMISR, and EISCAT have recorded long and extensive observations of meteors (Pellinen-Wannberg and Wannberg, 1994; Zhou QH et al., 2001; Mathews et al., 2008). Phased-array radar has obvious advantages over traditional ISR in meteor observation because of its flexible beam scanning.

In this experiment, we designed a special working mode to improve the ability of the radar to detect meteors. The radar beam was perpendicular to the magnetic field line at an altitude of 100 km. Specifically, the beam direction was 354° azimuth and 42° elevation locally. The pulse working mode was adopted, with a transmission bandwidth of 4 MHz, a pulse width of 200 μs, and a pulse repeating period of a 6.6 ms linear frequency modulation signal. The I/Q echo signal of each pulse was recorded. We developed an algorithm to identify and extract meteor parameters automatically. The specific parameters used for the meteor monitoring experiment are also shown in Table 2.

As an example, Figure 10 shows the range-time-intensity of three typical meteor echoes observed by the SYISR-8. In the left panel, the strong, oblique straight-line echo is the meteor head echo, which is the reflection echo of a meteoroid to the incident electromagnetic wave. The range extended echo, with a relatively lower

intensity and time delay to the head echo, is called the range-spread trail echo and is due to the scattering of plasma generated during meteor ablation (Dyrud et al., 2002). In the right panel, the echo with an almost constant range versus the observation time is called a specular trail echo or a constant range echo and is formed by a meteoroid perpendicular to the radar beam (Dyrud et al., 2002).

#### 4. Conclusions and Future Plans

We have built a prototype of SYISR consisting of eight subarrays (SYISR-8) to conduct experimental tests for the purpose of minimizing the technical risks that might arise by producing the entire array. Here we have summarized the main technical issues encountered when building the SYISR-8 and our preliminary experimental results. The main conclusions are as follows:

(1) The main components passed the extreme environment test. An indoor passive subarray was built to test the antennas. Its wide-angle scanning characteristic, stationary wave characteristic, and radiation pattern were confirmed to meet the design requirements. In addition, an indoor active subarray was built to test the performance of the system. The transmitting and receiving lobes were measured to determine the beam width and gain. The reliability and stability were confirmed through continuous operation for 60 hours.

(2) The amplitude and phase among 256 channels were calibrated through an embedded internal monitoring network. The mean oscillation of the amplitude and phase was about 1 dB and 5°, respectively, which met the basic requirements. The beam directivity was confirmed by crossing screen of the International Space Station.

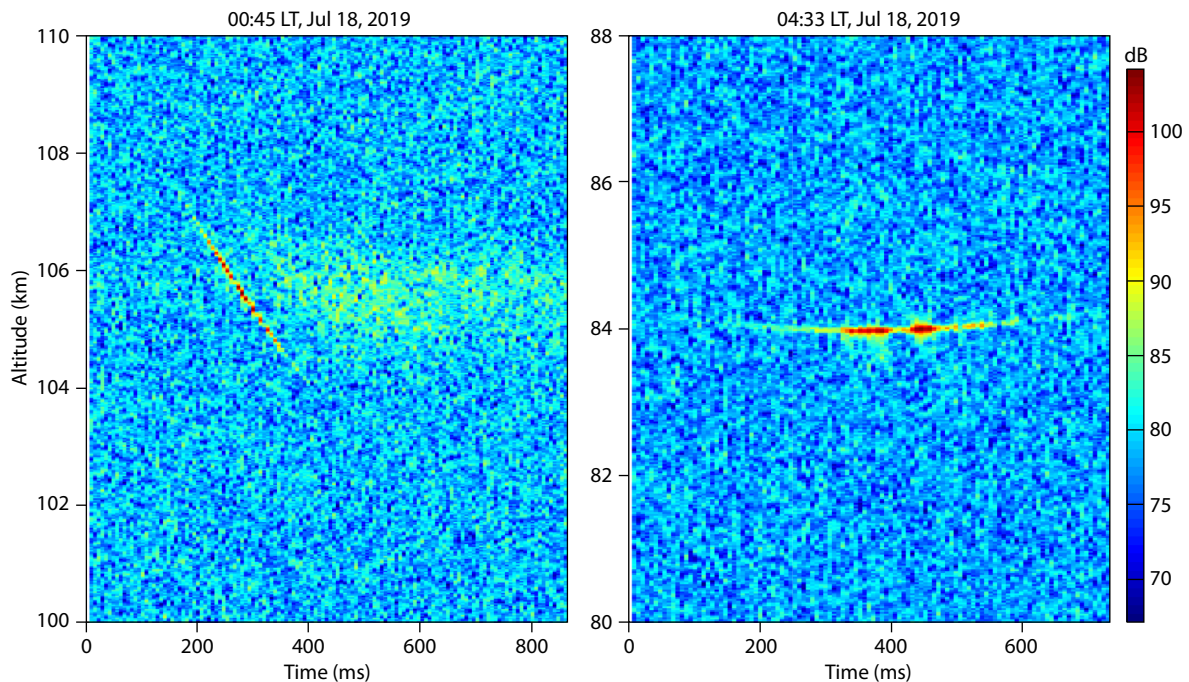


**Figure 10.** Range-time-intensity of the SYISR-8 signal during two meteor occurrences measured on July 18, 2019. The left panel shows the simultaneous occurrence of the meteor head echo and range-spread trail echo around local time 00:45. The right panel is a typical specular scattering echo that occurred around local time 04:33.

(3) The SYISR-8 was further configured to be able to detect tropospheric wind profiles and meteors. Several experiments were done in different seasons. An algorithm was developed to derive the tropospheric wind from SYISR-8 measurements. The derived winds were evaluated by comparison with independent radio-sonde and balloon-based GPS measurements. The SYISR-8 was able to observe several typical meteor echoes, such as the meteor head echo, range-spread trail echo, and specular trail echo.

These promising experimental results confirm the validity and reliability of the SYISR-8 system. They have reduced the technical risk of producing the entire large array of the SYISR to some extent. We are now moving toward building the full SYISR system, and we expect it to be completed by the end of this year. Furthermore, we have been funded by the Meridian Project II to extend the SYISR to become a tristatic ISR system. Specifically, we will double the power of the current SYISR array and build two additional remote receivers on Hainan Island. This will greatly enhance our ability to monitor the low-latitude ionosphere of China.

## Acknowledgments

This work was supported by the National Natural Science Foundation of China (grant no. 41427901) and the Strategic Priority Research Program of the Chinese Academy of Sciences (grant no. XDA17010206). We acknowledge the significant contributions of the engineering team from the Nanjing Research Institute of Electronics Technology beyond the author list. The experimental data can be obtained upon request through the corresponding authors.

## References

- Benjamin, S. G., Schwartz, B. E., Szoke, E. J., and Koch, S. E. (2004). The value of wind profiler data in U.S. weather forecasting. *Bull. Amer. Meteor. Soc.*, 85(12), 1871–1886. <https://doi.org/10.1175/BAMS-85-12-1871>
- Bowles, K. L. (1958). Observation of vertical-incidence scatter from the ionosphere at 41 Mc/sec. *Phys. Rev. Lett.*, 1(12), 454–455. <https://doi.org/10.1103/PhysRevLett.1.454>
- Cohen, M. H. (2009). Genesis of the 1000-foot Arecibo dish. *J. Astron. Hist. Heritage*, 12(2), 141–152.
- Ding, Z. H., Wu, J., Xu, Z. W., Xu, B., and Dai, L. D. (2018). The Qujing incoherent scatter radar: system description and preliminary measurements. *Earth, Planets and Space*, 70(1), 87. <https://doi.org/10.1186/s40623-018-0859-8>
- Dougherty, J. P., and Farley, D. T. (1960). A theory of incoherent scattering of radio waves by a plasma. *Proc. Roy. Soc. A*, 259(1296), 79–99. <https://doi.org/10.1098/rspa.1960.0212>
- Dyrud, L. P., Oppenheim, M. M., Close, S., and Hunt, S. (2002). Interpretation of non-specular radar meteor trails. *Geophys. Res. Lett.*, 29(21), 2012. <https://doi.org/10.1029/2002GL015953>
- Fukao, S., Sato, T., Tsuda, T., Kato, S., Wakasugi, K., and Makihira, T. (1985). The MU radar with an active phased array system: 1. Antenna and power amplifiers. *Radio Sci.*, 20(6), 1155–1168. <https://doi.org/10.1029/rs020i006p01155>
- Fulton, C., and Chappell, W. (2009). Calibration techniques for digital phased arrays. In *Proceedings of 2009 IEEE International Conference on Microwaves, Communications, Antennas and Electronics Systems* (pp. 1–10). Tel Aviv, Israel: IEEE. <https://doi.org/10.1109/COMCAS.2009.5385979>
- Gordon, W. E. (1958). Incoherent scattering of radio waves by free electrons with applications to space exploration by radar. *Proc. IRE*, 46(11), 1824–1829. <https://doi.org/10.1109/JRPROC.1958.286852>
- Hagfors, T. (1961). Density fluctuations in a plasma in a magnetic field, with applications to the ionosphere. *J. Geophys. Res.*, 66(6), 1699–1712. <https://doi.org/10.1029/JZ066i006p01699>
- Kudeki, E., and Milla, M. A. (2011). Incoherent scatter spectral theories—Part I: a general framework and results for small magnetic aspect angles. *IEEE Trans. Geosci. Remote Sens.*, 49(1), 315–328. <https://doi.org/10.1109/TGRS.2010.2057252>
- Kuehnle, L. (2001). Phased array calibration procedures based on measured element patterns. In *Proceedings of the 2001 11th International Conference on Antennas and Propagation* (pp. 660–663). Manchester, UK: IEEE. <https://doi.org/10.1049/cp:20010372>
- Lindseth, B., Brown, W. O. J., Jordan, J., Law, D., Hock, T., Cohn, S. A., and Popovic, Z. (2012). A new portable 449-MHz spaced antenna wind profiler radar. *IEEE Trans. Geosci. Remote Sens.*, 50(9), 3544–3553. <https://doi.org/10.1109/TGRS.2012.2184837>
- Liu, J. X., Yu, X., Liang, C. J., Sun, K., and Sun, H. J. (2011). Calibration method of amplitude and phase consistency of digital variable polarization radar receiving system. In *Proceedings of 2011 IEEE International Conference on Microwave Technology & Computational Electromagnetics* (pp. 44–47). Beijing, China: IEEE. <https://doi.org/10.1109/ICMTCE.2011.5915162>
- Mailoux, R. J. (2005). *Phased Array Antenna Handbook* (2nd ed). Boston: Artech House.
- Mathews, J. D., Briczinski, S. J., Meisel, D. D., and Heinselman, C. J. (2008). Radio and meteor science outcomes from comparisons of meteor radar observations at AMISR poker flat, sondrestrom, and Arecibo. *Earth Moon Planets*, 102(1–4), 365–372. <https://doi.org/10.1007/s11038-007-9168-0>
- McCrea, L., Aikio, A., Alfonsi, L., Belova, E., Buchert, S., Clilverd, M., Engler, N., Gustavsson, B., Heinselman, C., ... Vierinen, J. (2015). The science case for the EISCAT\_3D radar. *Prog. Earth Planet. Sci.*, 2(1), 21. <https://doi.org/10.1186/s40645-015-0051-8>
- Pellinen-Wannberg, A., and Wannberg, G. (1994). Meteor observations with the European incoherent scatter UHF radar. *J. Geophys. Res.*, 99(A6), 11379–11390. <https://doi.org/10.1029/94ja00274>
- Röttger, J., and Liu, C. H. (1978). Partial reflection and scattering of VHF radar signals from the clear atmosphere. *Geophys. Res. Lett.*, 5(5), 357–360. <https://doi.org/10.1029/gl005i005p00357>
- Röttger, J., Wannberg, U. G., and van Eyken, A. P. (1995). The EISCAT scientific association and the EISCAT Svalbard radar project. *J. Geomag. Geoelectr.*, 47(8), 669–679. <https://doi.org/10.5636/jgg.47.669>
- Strauch, R. G., Merritt, D. A., Moran, K. P., Earnshaw, K. B., and van de Kamp, D. (1984). The Colorado wind-profiling network. *J. Atmos. Oceanic Technol.*, 1(1), 37–49. [https://doi.org/10.1175/1520-0426\(1984\)001<0037:TCWPN>2.0.CO;2](https://doi.org/10.1175/1520-0426(1984)001<0037:TCWPN>2.0.CO;2)
- Thomson, J. J. (1906). *Conduction of Electricity Through Gases*. Cambridge: Cambridge University Press.
- Valentic, T., Buonocore, J., Cousins, M., Heinselman, C., Jorgensen, J., Kelly, J., Malone, M., Nicolls, M., and van Eyken, A. (2013). AMISR the advanced modular incoherent scatter radar. In *Proceedings of 2013 IEEE International Symposium on Phased Array Systems and Technology* (pp. 659–663). Waltham, USA: IEEE. <https://doi.org/10.1109/ARRAY.2013.6731908>
- Zeng, L. Q., and Yi, F. (2011). Lidar observations of Fe and Na meteor trails with high temporal resolution. *J. Atmos. Solar Terr. Phys.*, 73(16), 2367–2372. <https://doi.org/10.1016/j.jastp.2011.08.002>
- Zhou, Q. H., Mathews, J. D., and Nakamura, T. (2001). Implications of meteor observations by the MU radar. *Geophys. Res. Lett.*, 28(7), 1399–1402. <https://doi.org/10.1029/2000GL012504>